Stabilising transient ferromagnetic states in nanopatterned FeRh with shape-induced anisotropy

Journal Article

Author(s):
Grimes, Michael; Sazgari, Vahid; Parchenko, Sergii; Zhou, Jingyuan; Soh, Yona; Heyderman, Laura J.; Thomson, Thomas; Scagnoli, Valerio

Stabilising transient ferromagnetic states in nanopatterned FeRh with shape-induced anisotropy

M Grimes[1,2,3,4,*] , **V Sazgari**[3], **S Parchenko**[2,3,5] , **J Zhou**[2,3], **Y Soh**[3], **L J Heyderman**[2,3] , **T Thomson**[1] **and V Scagnoli**[2,3,*]

[1] NEST, Department of Computer Science, The University of Manchester, Oxford Road, Manchester M13 9PL, United Kingdom
[2] Department of Materials, Laboratory for Mesoscopic Systems, ETH Zurich, 8093 Zurich, Switzerland
[3] Paul Scherrer Institute, 5232 Villigen PSI, Switzerland

E-mail: michael.grimes@esrf.fr and valerio.scagnoli@psi.ch

CrossMark

Abstract

It is well-known that FeRh undergoes an antiferromagnetic to ferromagnetic (FM) phase transition where the high temperature phase is a low coercivity FM material. However, little is known about the effect of lateral confinement on the transition dynamics in FeRh thin films. Here, we pattern FeRh thin films into arrays of nanowires with a large aspect ratio (100:1) and, with ultrafast probing of the magnetic state in an applied magnetic field, we determine the influence of demagnetization fields on the stability of laser induced FM domains. In particular, with pump-probe Kerr measurements, we demonstrate that, when a magnetic field is applied along the nanowire length, the nanowire arrays exhibit an FM phase (>3.0ns) that is longer-lived than that observed for continuous thin films (≈2.0 ns). With electrical measurements, we also show that the transition temperature depends on the relative orientation of the magnetic field. Indeed, when the FeRh film is patterned with sub-μm features, the transition temperature decreases by up to 7 K depending on the field direction at applied magnetic fields of 1 T. The effects of sample heating are explored using finite-element simulations to determine the heat dissipation following laser excitation across a range of FeRh nanowire widths. These simulations confirm that the increased lifetimes of the magnetic-field-aligned FM domains in the nanowire arrays are not due to differences in heat dissipation. This suggests that FM domain growth and relaxation through the ultrafast phase transition in FeRh nanowires is strongly dependent on the shape anisotropy. This knowledge is important for the fine control of the phase transition in patterned FeRh thin films for nanoscale devices.

[4] Current Address: ESRF, 71 Av. des Martyrs, 38 000 Grenoble, France.
[5] Current Address: European XFEL, Holzkoppel 4, 22 869 Schenefeld, Germany.
[*] Authors to whom any correspondence should be addressed.

(Some figures may appear in colour only in the online journal)

1. Introduction

The control of magnetic phase transitions is of key interest across a wide range of applications [1], with the most commercially relevant being those in the field of magnetic data storage [2, 3]. Magnetic phase transitions offer a method of switching magnetic states with lower total energy cost than current technologies when implemented in emerging schemes such as heat-assisted magnetic recording (HAMR) [3, 4]. $Fe_{50}Rh_{50}$ in the B2 crystallographic phase has become an archetype for studying such magnetic phase transitions due to the transition temperature being readily accessible under normal laboratory conditions ($T_T \sim 380$ K [5]). As part of this transition, the Fe atomic spins reorientate, going from an antiferromagnet (AF) [6] to a ferromagnet (FM) [7] on increasing the temperature. The FM ordering of Fe spins further induces a moment on the associated Rh atom [8] increasing the total magnetic moment of the unit cell (see figure 1(a)) [9].

FeRh has also attracted attention as a result of the coupling between the electronic, spin, and lattice degrees of freedom across the phase transition. In particular, the change in magnetic order is accompanied by a transformation of electronic structure, which reduces the resistivity by 33% [10, 11], and there is also an isotropic expansion of the crystal lattice volume by 1% where the ordered bcc (B2, CsCl-type) structure is maintained [12]. As a result of these coupled physical phenomena in FeRh, the modulation of the transition temperature (T_T) can arise from a wide variety of factors [13]. This is because the AF and FM ground states are relatively close in energy as demonstrated by *ab initio* and atomistic simulations [14–16]. Hence, a small perturbation that stabilises either state can alter T_T as well as the distribution of transition temperatures (ΔT). Indeed, it is known that T_T is sensitive to both long-range and short-range structural distortions [16, 17], and interfacial strain can affect the transition properties via the choice of capping layer [18], or the substrate [17]. When a tensile strain is imposed on the FeRh film (*e.g.* through epitaxial growth on MgO) the FM state is accessed at lower temperatures [19]. While this effect is more pronounced in thinner films (<10 nm) [19, 20], permanent FM interfacial layers are also reported in thicker FeRh films (100 nm) [21–23]. Increases in local disorder can further promote the stabilisation of FM behaviour by inducing the disordered fcc (A1) phase of FeRh [16], which is FM across all temperatures. With the implementation of ion-irradiation, the sensitivity of this A1 state has been demonstrated, which can be selectively induced as a function of film depth [21, 24]. Extrinsic factors, such as an applied magnetic field, will also influence T_T, where the energy barrier for the transition to the FM state

can be modified. It has been reported that there is a reduction in T_T under the application of strong magnetic fields [23, 25], exhibiting a field dependence of T_T of $\approx$9 K T^{-1}. This is understood by considering the effect of field induced spin canting of the Fe in the AF phase, where simulations have indicated a reduced energy barrier to spin re-orientation [26, 27].

Patterning FeRh thin films into nanostructures provides a mechanism whereby substrate-induced strain is mitigated by strain relief at feature edges [28, 29]. However, nanoscale sample damage (a by-product of the ion milling process) close to patterned feature edges (within 100's nm) must also be considered [28]. In addition to a shift in T_T in FeRh nanowires, an asymmetric phase transition has also been observed [30]. Specifically, the FM $\rightarrow$ AF reverse transition exhibited a narrower ΔT with step-like behaviour in comparison to the smooth AF $\rightarrow$ FM transition. Uhlíř *et al* [30] speculated that the applied magnetic field is enhanced by a significant demagnetization field in the nanowires. This demagnetization field is reduced when FM domains begin to relax to the AF phase, resulting in a sharper transition behaviour upon cooling. Indeed, the switching of individual domains are observed with step-like changes in electrical resistivity.

Despite the large body of work on FeRh thin films, the effect of lateral confinement on the transition dynamics remains under-reported. The dynamics of the FeRh phase transition have been explored with probing of the electronic [15], magnetic [31, 32], and lattice [33] transformations across a range of timescales from sub-ps [15] up to ns [34, 35]. It is known that the AF $\rightarrow$ FM transition mechanism differs from the reverse transition as a consequence of the different domain sizes (AF domain sizes are <100 nm, while FM domain sizes $\approx$1 μm) [36–38]. The FM domains are established through a nucleation-growth process while AF domains require only nucleation [37]. The modification of T_T arising from the shape anisotropy [30] and the lithography-induced structural disorder [28] is expected to alter the switching behaviour according to previous reports of the FeRh phase transition [13, 16]. When the size of the patterned elements approaches the domain size of the FM phase, it is expected that the sample demagnetization field can affect the transition behaviour, as has been demonstrated in static measurements [30].

Here we report on time-resolved magneto-optic Kerr effect measurements (TR-MOKE) of the magnetization dynamics across the phase transition of patterned arrays of FeRh nanowires. The wire length provides the dominant easy axis along which to align the magnetization assuming
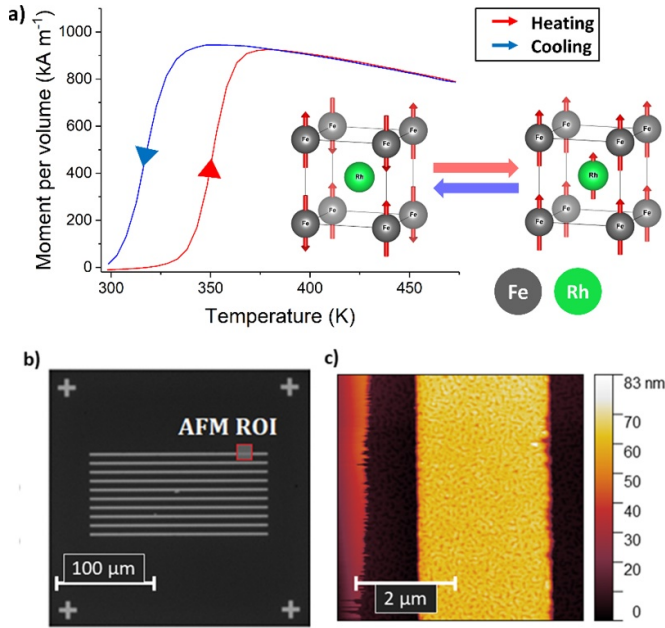
J. Phys. D: Appl. Phys. **56** (2023) 485002

M Grimes *et al*

Figure 1. (a) Magnetometry performed on the FeRh thin film sample at an in-plane applied field of 1000 Oe. The AF → FM transition upon heating is seen where the magnetization increases at around 355 K. The corresponding spin configuration of the system in each phase is provided (inset). (b) Optical microscope image of nano-patterned wire array with wire width of 2.5 μm. (c) Atomic force microscopy image of the surface is provided for the marked region of interest (ROI) in part b. The roughness (root-mean square) of the shown nanowire surface was 2.3 nm.

an insignificant in-plane (IP) magnetocrystalline magnetic anisotropy [39]. Samples with a large shape anisotropy show a sensitivity to the direction of the applied magnetic field, with increased lifetimes of FM states observed for smaller demagnetization fields. Simulations of heat dissipation and static electrical measurements confirm that the increased stability of the FM phase in the nanowire arrays is a result of the smaller demagnetizing fields associated with the nanowire shape.

2. Methods

$Fe_{50}Rh_{50}$ (30 nm) thin films were dc magnetron sputter deposited on to MgO(001) substrates and capped with a 3 nm thick Pt layer to inhibit the formation of surface oxides [22]. The Pt layer is deposited at room temperature to minimize the probability of Pt interdiffusion. The details of the sputter parameters for the FeRh thin films can be found in previously published work [17, 22]. The film was characterised by x-ray diffraction (XRD), x-ray reflectivity (XRR), and vibrating sample magnetometry to confirm the expected crystal structure, lattice expansion, and magnetic transition present in these samples (see supplementary material). B2 order is confirmed by the observation of FeRh (001) and (002) XRD peaks. From the relative intensity of these peaks, a structural order parameter, $S = 0.8$ is obtained, demonstrating good crystallographic quality [40]. The XRR data (supplementary material) confirms that Pt from the capping layer does not measurably interdiffuse into FeRh. The expected AF → FM transition was

observed on heating with $T_T = 353$ K and $\Delta T = 25$ K (red curve in figure 1(a)).

The FeRh thin films were subsequently patterned into arrays of nanowires with wire widths ranging from 2.5 μm down to 300 nm. The period of the arrays (nanowire centre-to-centre distance) was four times that of the wire width, and the number of wires in each array varies from 10 (in the case of 2.5 μm wires; see figure 1(b)) up to 80 (0.3 μm wires). A Vistec EBPG 5000Plus electron-beam writer was used to prepare resist masks with electron-beam lithography. Following development, the nanowire arrays were created by Ar^+ ion-milling using an Oxford Ionfab 300Plus. Edge damage was limited through the use of a relatively low acceleration voltage (300 V) of the ions during the milling process with the purpose of minimising changes in T_T arising from structural disorder [16, 28]. The quality of the resulting nanowire surfaces are verified with a surface roughness of 2.3 nm as measured by atomic force microscopy; see figure 1(c). A dielectric layer was subsequently deposited to enhance the Kerr signal in pump-probe experiments by acting as a resonant cavity for light at a wavelength of 1030 nm [41]. Further details are available in supplementary material.

Measurements of the magnetization dynamics in the thin films and nanowire arrays were performed using a lab-based TR-MOKE system; see figure 2(a). For these measurements, the sample was excited by a 150 fs laser pulse with laser wavelength $\lambda = 515$ nm at a fluence of 4.0 mJ cm^{-2} and a repetition rate of 200 kHz, before being probed with a low fluence pulse ($\lambda = 1030$ nm) [42]. The Kerr rotation at fixed pump-probe delays was measured while sweeping the applied magnetic field between -110 and $+110$ mT. The FeRh samples were automatically re-initialised to an AF state after each laser pump event [43] as the laser repetition rate (200 kHz) allows sufficient time for the sample to disperse the laser energy and to return to thermal equilibrium.

In order to estimate the lifetime of the FM state in the FeRh systems, finite-element modelling of the heat dissipation was undertaken using COMSOL®. To model the width of the transition conductivity, heat capacity, density, and Young's modulus are allowed to change gradually about T_T using an error function with FWHM equal to the experimentally determined ΔT [29]; see figure 1(a). To determine the rate of heat loss to the MgO substrate, the interfacial heat transfer coefficient, κ_{IF}, was first estimated [44, 45]. Then the parameter κ_{IF} was varied until the temperature profile of the film as simulated in COMSOL® exhibited a relaxation profile comparable to the TR-MOKE results over the 2–5 ns timescale; see figure 2(c). The finite-element modelling simulation tracks the evolution of the lattice expansion. As such, transient changes in volume were used as a measure of the FM phase percentage as the system relaxes since the lattice and spin systems are assumed to be fully coupled in this regime [46].

A physical property measurement system (PPMS) was used to probe resistivity. Contact pads, which spanned all wires in the arrays, were fabricated enabling electrical connections to be made. The measurements were performed using a standard four-point probe methodology (see supplementary material). The resistance of the nanowire arrays was measured under
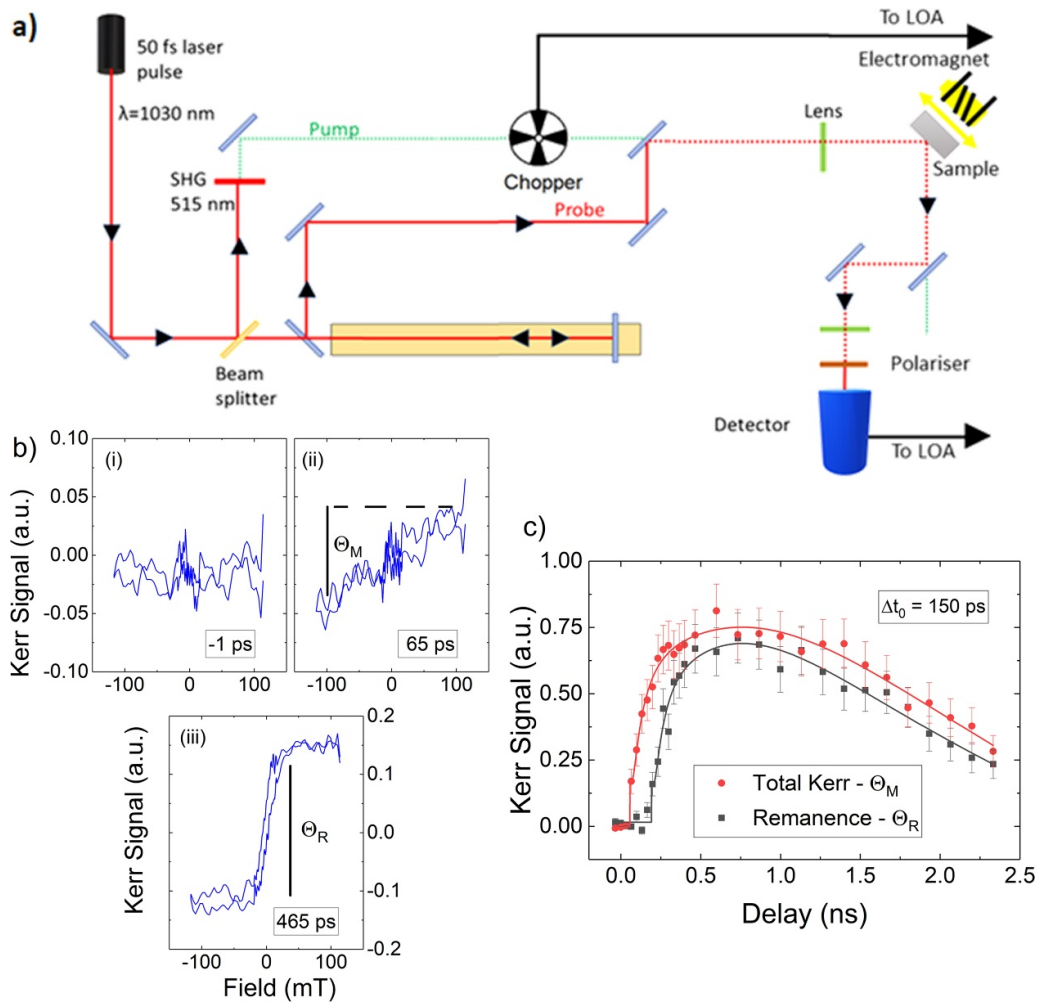
Figure 2. (a) Schematic of the laser system used to perform the pump-probe Kerr measurements. The lock-in amplifier (LOA) is triggered by the chopper with a rotational frequency of 1 kHz. The Kerr rotation is measured as both a function of probe delay and applied field strength. (b) The magnetic response of FeRh thin films at different times on application of magnetic fields between +110 and −110 mT: (i) at negative time delay, no signal is observed. At positive time delays, the response changes from a linear response (ii), to one at later times that saturates under magnetic field (iii). Kerr rotation, Θ_M, and remanence, Θ_R, are extracted from linear fits to the data. (c) Plot of Kerr signal and remanence as a function of pump-probe delay. The delay in the rise time of Θ_R after excitation is evident from the fitting of the data using a growth and decay model; a delay time of 150 ps for Θ_R to emerge is found. The Θ_M and Θ_R growth rates are similar.

zero field (ZF) and in an applied magnetic field of 1 T, which was applied both axially IP, parallel to the wire length, and out-of-plane (OOP). In each case, the sample was heated in a cycle; $300 \rightarrow 400 \rightarrow 300$ K, with constant applied field of 0 or 1 T maintained throughout. Transition fields were measured by performing isothermal field sweeps from +9 T to −9 T at temperatures that span the FeRh phase transition. Isothermal field sweeps were performed for both axial IP and OOP orientations of the magnetic field.

3. Results and discussion

3.1. Magneto-optical investigation of phase transition in patterned FeRh

The laser-induced AF $\rightarrow$ FM phase transition of FeRh has been well documented in the literature, where magnetic order evolves over hundreds of ps before micrometre-scale FM

domains are established [28, 32]. However, the effect of applied magnetic fields on the progression to the FM phase has only recently been explored [47]. It is also well known that the transition temperature is dependent on the strength of the applied field exhibiting a shift to lower temperatures at a rate of 9 K T^{-1} [23]. Furthermore, in FeRh samples with significant IP shape anisotropy, it has been shown that the application of a magnetic field parallel to the IP easy axis has the effect of stabilizing the FM phase [27]. Here, we extend this work to shorter time scales using a pump-probe technique, with TR-MOKE experiments performed on arrays of nanowires (see figure 1(b)) under different applied magnetic fields and at a fixed temperature (RT $\approx$ 295 K). The full experimental details can be found in the methods section.

3.1.1. Dynamic evolution of Kerr signal in FeRh thin films.
The transient magnetic properties of FeRh thin films following laser excitation are first determined. We identify three stages in

the Kerr response through the laser-induced AF → FM phase transition; see figure 2(b). Before laser excitation, the Kerr signal shows no response to field. This is consistent with the AF phase. For the 150 ps following excitation, a linear relationship with field (up to 110 mT) is seen. This is quantified from the peak-to-peak value across the field applied, referred to as Θ_M. After 150 ps have elapsed, it is observed that the Kerr signal saturates above certain magnetic field strengths. This is expected when the sample has transitioned to the FM phase, considering the soft nature of the FeRh in this state. The positive and negative saturated response is fit for both the positive and negative applied magnetic fields to estimate the height of the hysteresis loop at ZF, which we call the Kerr remanence, Θ_R. It should be noted that, with such a dynamic probe, information about the transient coercivity is unavailable due to relaxation to the AF phase between laser pulses [48]. As seen in figure 2(c), the Kerr and remanence signals exhibit slightly different transitory behaviour. The Kerr signal, Θ_M, increases rapidly after excitation showing maximum response within 500 ps. In contrast, Θ_R is slower to emerge, appearing 150 ps after excitation, with the maximum value in Θ_R observed after 700 ps. In order to model this behaviour, the transition is quantified by adapting the traditional growth-decay model [31] to include a time delay:

$$\Theta(t) = G(t) \cdot \left[A \left(1 - e^{-(t-t_0)/\tau_G} \right) + B \left(e^{-(t-t_0)/\tau_R} \right) \right], \tag{1}$$

where $\Theta(t)$ is the transient Kerr signal, τ_G and τ_R are the respective growth and decay lifetimes, and t_0 is the time delay for the signal to emerge. When this model is applied to the Θ_M signal (where t_0 is assumed to be 0), we find that sample magnetization quickly grows with a growth lifetime, $\tau_G = 75$ ps. The rapid initial increase in the Θ_M signal seen in figure 2(c) would suggest the emergence of small FM regions within some fraction of the sample in a matter of ps, consistent with results seen in recent x-ray absorption spectroscopy studies [49]. The signal shows no remanence in this time frame, which is likely to be due to the presence of regions with randomly oriented magnetization and high coercive field. In contrast, Θ_R has a delay, t_0, of 150 ps, whilst possessing a similar τ_G. This signal tracks the growth of FM regions with magnetization aligned to the field within the probed area. The measured lifetimes are consistent with previous x-ray magnetic circular dichroism (XMCD) studies [9]. The XMCD results showed that the initial formation of FM regions occurs within 100 ps but domains with μm size are established over a timeframe of several ns [36]. We have also estimated the magnetization (Θ_M) decay lifetimes to be 2.7 ns; see figure 2(c). This value is in good agreement with values reported in the x-ray photoemission electron microscopy work of Ünal *et al* [35]. Specifically, by tracking the spatial extent of FM domains as a function of probe delay (with a time resolution of 50 ps), they observed that relaxation occurred over 2 ns, consistent with the timescale of heat dissipation in metals. The agreement with previous pump-probe experiments is strong evidence that we

can track the growth and decay of FM domains with the Θ_M and Θ_R values.

3.1.2. Dynamics of patterned FeRh nanowire arrays in an axial magnetic field. In this section, we report the growth dynamics of FM domains in patterned samples. The pump-probe measurements performed on the thin films in the previous section were repeated for the series of nanowire arrays described in the methods section. The IP magnetic state was monitored by measuring the longitudinal Kerr response. Initially, the experiment is performed with the magnetic field applied parallel to the wire length; see figure 3(a). This magnetic field orientation is referred to as the axial field throughout this work. Under an axial field, the array of 2.5 μm wide nanowires exhibits a Θ_R that peaks within 400–500 ps and does not decay appreciably over the 2.5 ns timescale investigated; see figure 3(b). This is similar to the dependence seen for the thin films; see Θ_R in figure 2(c). Considering the demagnetising field, we have estimated that the applied magnetic field strengths should be sufficient to saturate the magnetic moment of the soft FM phase (coercivity, $\mathbf{H}_c < 30$ mT [7]).

The results from our series of nanowire arrays are shown in figure 3, where the wire width varies from 0.3 to 2.5 μm. The FM-type behaviour, with a rapid increase in the Θ_M, is observed across the range of wire widths for an axial magnetic field. The maximum signal emerges within 0.5 ns and possesses lifetimes 2–3 times longer than those seen for FeRh thin films of the same thickness (compare figure 3 with figure 2). The entire range of the lifetimes extracted from fitting equation (1) to the Θ_R data is available in supplementary material. Since the time delay between Θ_R and Θ_M is still 100–200 ps, this indicates that the mechanism for aligning the magnetization in the FM domains to the magnetic field is similar to that for thin films. This agrees with previous dc electrical measurements where the AF → FM transition did not differ from that seen in thin film samples [30].

3.1.3. Dynamics of patterned FeRh nanowire arrays in a tangential magnetic field. The behaviour is expected to significantly change when the magnetic field is applied in the plane of the sample but perpendicular to the wire length. This is because a greater demagnetization factor would result in a reduced total effective field. Indeed, the demagnetising fields are expected to cause a transition asymmetry in FeRh nanowires [30]. In particular, applying the magnetic field along the short axis of the wires in the patterned sample is expected to increase the barrier for the phase transition for a fixed applied field strength. This is due to the well-known relationship between T_T and the magnetic field strength, where an increase of 1 T reduces the transition temperature by 9 K [23].

The effect of the demagnetising field was therefore determined by performing pump-probe measurements with the field applied orthogonal to the wire widths, in the plane of the sample [50]. This is termed the tangential configuration. We report the longitudinal Kerr response as before, with applied magnetic field strengths up to 110 mT.
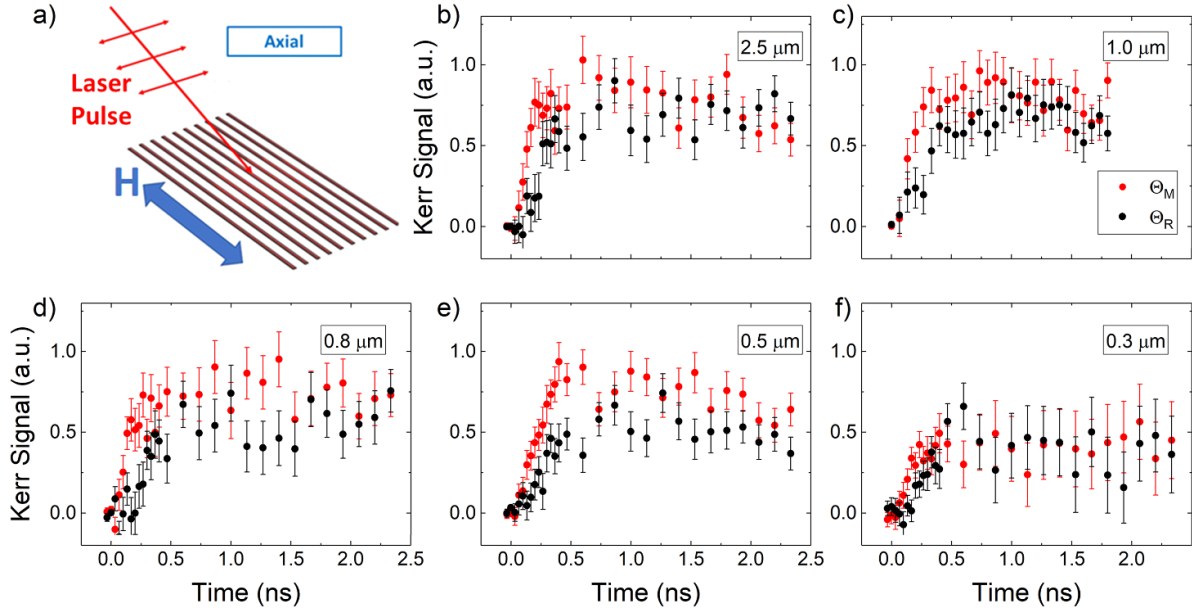
Figure 3. (a) Experimental geometry for the axial MOKE experiment. The blue double-headed arrow indicates the applied magnetic field direction; the longitudinal Kerr signal was probed. (b)–(f) Θ_M and Θ_R as a function of pump-probe delay under an axial applied field for the range of nanowire arrays probed. The scans are arranged in descending order of wire width, from 2.5 to 0.3 μm. Θ_R is found to persist over longer timescales than seen for FeRh thin films of the same thickness.

The different responses of 2.5 μm nanowires on applying the magnetic field axially and tangentially are seen by comparing the FM relaxation dynamics in figures 3(b) and 4(b). In contrast to the axial case, the tangential configuration TR-MOKE scans exhibit a reduced Θ_R that appears within 500 ps but relaxes back to zero within the time frame of the scan (<2.5 ns). As seen in figure 4, under a tangential magnetic field, the nanowire arrays display a reduced Θ_R, both in magnitude and lifetime, which reduces as the wire width decreases. The arrays with the narrowest 0.5 and 0.3 μm nanowires exhibit almost zero Θ_R. In all instances, Θ_M is observed but exhibits faster relaxation to the ambient state than seen for an axial magnetic field. This would indicate a reduced stability of field-aligned FM phase for the measured tangential fields (up to 110 mT). The absence of Θ_R in the thinnest nanowire arrays is attributed to the large fields required to align the magnetization of the FM domains in this direction, while the measurable Kerr signal, Θ_M, suggests that the magnetic phase transition still occurs. In order to understand the origin of the longer-lived remanence in the nanowire arrays (figure 3) when compared to the thin films (figure 2), finite-element modelling is used to determine any differences in the propagation of heat through FeRh nanostructures following laser excitation.

3.2. Finite-element modelling of heat dissipation in FeRh thin films and nanowire arrays

Slow relaxation to ambient temperatures is one potential mechanism that would explain the longer-lived FM state observed in the nanowire arrays. Therefore, in order to understand the role of heat dissipation in the dynamics of the FeRh

phase transition in thin films and nanowire arrays, the heat transfer within FeRh films grown on MgO substrates was modelled with the COMSOL® finite-element modelling software.

As a result of the coupling between the electronic, spin, and lattice degrees of freedom across the phase transition in FeRh [13], the evolution of the system into the FM state can be probed (and simulated) with a range of physical transformations. For example, the isotropic lattice expansion can indicate when the FM state is reached, assuming the phonon and spin transformations are fully coupled. In modelling the heat dissipation in metals, which occurs over ns, we assume the lattice and the magnetic moments are fully coupled. Recent double-pump THz emission studies indicate that a time interval of $\approx$10 ps exists between the spin and lattice transformations [47] limited by the speed of sound. Therefore, our finite-element modelling focuses on local isotropic expansion, where the normalised density change is a measure of the FM state as a function of time. In figure 5(a), an example is shown of a 2D plot of material density 50 ps after a simulated laser pulse illuminates the central region. A series of simulations are conducted for FeRh thin films together with arrays of 2.5, 1.0, and 0.5 μm wide wires. The heat dissipation of a smaller 'patch' of FeRh thin film with surface area 100×200 μm^2, which is the same overall size as each of the nanowire arrays, was also simulated using a similar mesh to eliminate modelling artefacts. This allows a comparison between the rate of thermal dissipation found in each system. The laser heating was similar to that used in the experiment with a fluence of 4 mJ cm^{-2} and a beamwidth (1/e intensity) of 40 μm. The normalised change in density for each simulation is shown in figure 5. These results demonstrate that equilibrium temperatures (RT)
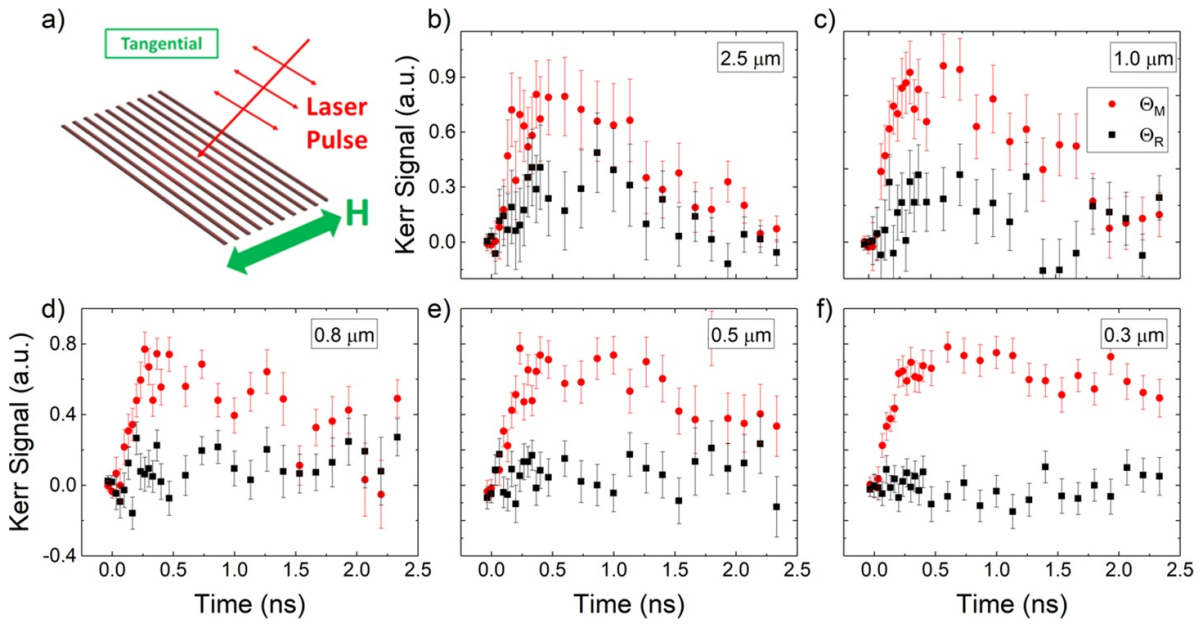
Figure 4. (a) Experimental conditions for the tangential geometry Kerr rotation measurements. The magnetic field is applied orthogonal to the long axis of the nanowires, and the longitudinal Kerr signal is probed. (b)–(f) The total Kerr signal, Θ_M, for all nanowire arrays (presented in descending order of nanowire width) exhibits growth decay dynamics similar to that of the thin film seen in figure 2(c). In addition, the FM remanence signal, Θ_R, has a decreased response when compared to that of the axial field configuration. Θ_R depends on the nanowire width, disappearing as the nanowires become thinner. The arrays with 0.5 and 0.3 μm nanowire widths present Kerr signals with negligible remanence signal.
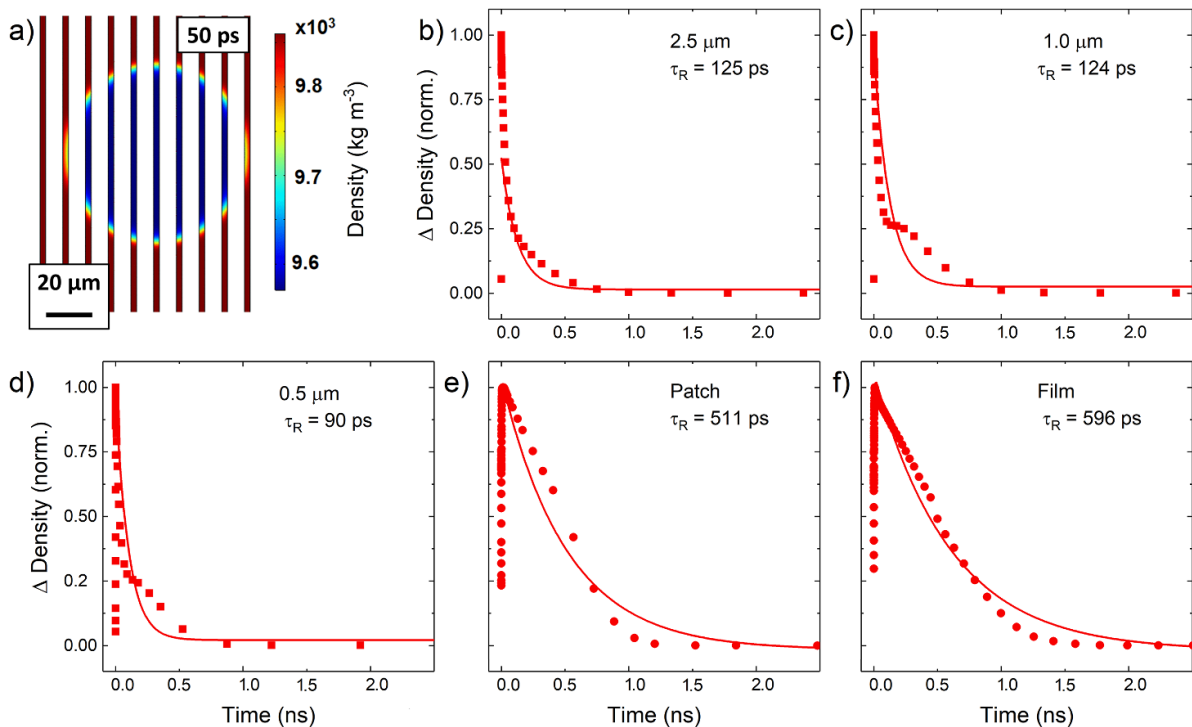

Figure 5. (a) Snapshot of density from COMSOL-simulated FeRh nanowire array (with nanowire width of 2.5 μm) 50 ps after laser excitation. The FM phase is assumed to correlate with lower density (blue) regions of the sample that occurs due to the lattice expansion. (b)–(d) Normalised density changes across the simulated FeRh nanowire arrays. (e)–(f) Normalised density changes of simulated FeRh patch (100×200 μm^2) and thin film. By fitting the dynamics with a growth decay model based on equation (1), it is seen that, in all instances, the nanowire array samples relax to the ambient state more quickly than the film and the patch, where decay rates are increased by a factor of 4.
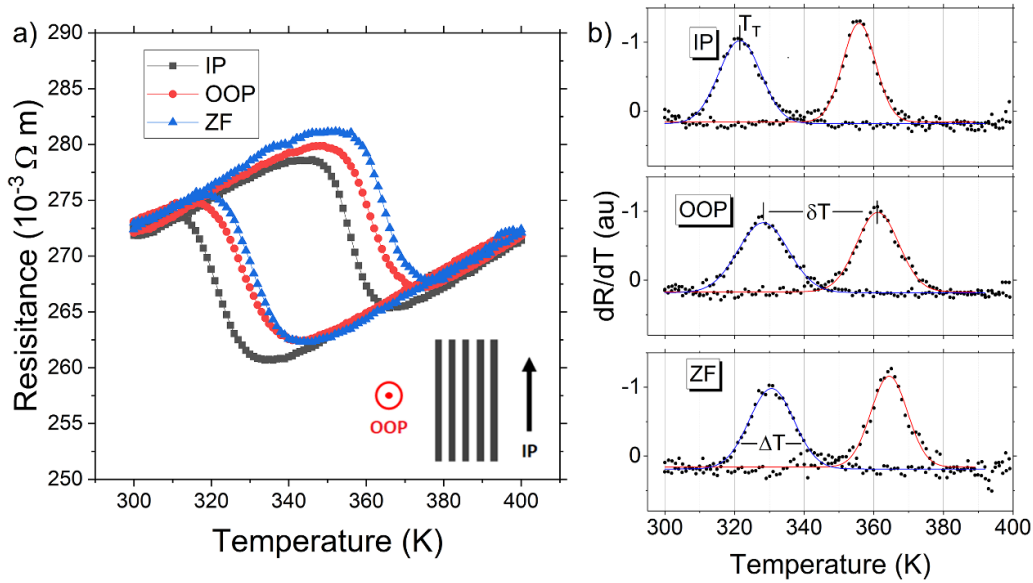
J. Phys. D: Appl. Phys. **56** (2023) 485002

M Grimes *et al*

Figure 6. Resistance as a function of temperature for FeRh array of 1 μm-wide nanowires. This was performed for three magnetic field configurations: ZF, axial IP, and OOP. The inset shows the different orientations of the applied field with magnitude 1 T. (b) T_T, ΔT, and δT were extracted in each case by fitting the first derivative of the heating (red) and cooling (blue) curves with Gaussian functions.

are reached within 2 ns in all instances. The finite-element modelling simulations predict that the temperature of the thinner wires will undergo a faster equilibration to ambient temperatures than thin films in such experiments, where the relaxation lifetimes are reduced by a factor of 4. The film and patch are almost identical in behaviour, indicating that the differences in dynamics of the simulations are not due to differences in lateral heat transfer processes. This would suggest that the heat dissipation is dominated by interfacial heat transfer.

The increase in the rate of heat dissipation in nanowires may be interpreted by considering the smaller, fractured surface area. Each wire has a larger effective heat sink in the form of bare MgO substrate at the wire edges. The MgO substrate absorbs some energy from the laser but the physical properties of the ceramic result in a reduced absorption in comparison to the metal [44]. While the increased initial temperature of the substrate will reduce the rate of heat transfer, the simulations indicate the heat sink effect, where the heat is more efficiently transferred from the nanowire arrays to the surrounding substrate, is more important for the dissipation of thermal energy. Indeed, it can be seen in figure 5 that the lower overall heat energy in nanowire arrays following laser excitation is easily dissipated to the MgO substrate and air within 1 ns. From this analysis, we must discount the hypothesis that a difference in transient FM behaviour of nanowire arrays is due to a reduced ability to transfer heat, when compared to thin metallic films. Indeed, these simulations predict that overall, heat dissipates more efficiently in the nanowire arrays than in the film, which would give reduced FM lifetimes if the average temperatures were the only criteria for the transition dynamics. Considering an interval between laser pulses of 5 μs (repetition rate = 200 kHz), this demonstrates that the longer-lived FM states observed in figure 3 are not due to poor heat dissipation.

3.3. Static electrical characterisation of FeRh nanostructures

In order to understand the effect of the demagnetization field on the phase transition in the FeRh nanowire arrays, we measure the resistance of individual arrays to estimate the transition temperatures; see figure 6(a). This is performed under an applied magnetic field, employing the two extreme cases: that of the axial IP and the OOP field orientations, which will give the strongest contrast in demagnetization field strength. Initially, the transition temperature was characterised at ZF to determine if there was a reduction in T_T for the nanowire arrays. This has been previously observed in FeRh nanoislands, arising from structural disorder that is a consequence of the lithography processes [28]. Next, by probing the applied magnetic field required to induce the lower resistivity FM phase, we estimate the net field experienced by the nanowires for a range of field configurations.

3.3.1. Resistance vs temperature curves. The coupled transition of FeRh allows for local investigations of T_T on patterned samples [29] with the measurement of the resistance, since the FeRh electronic band structure is modified as FeRh transforms from AF →FM magnetic order and this is associated with a change in resistivity of 33% [23]. Similar to the treatment of the magnetometry data in figure 1(a), T_T is defined as occurring at the maximum of the dR/dT curve, see figure 6(b). The phase transition, as tracked by resistance, displays a thermal hysteresis of $\delta T \approx 33 - 35$ K, indicative of a first order phase transition. Both T_T and the transition width agree with that found for the thin film from the magnetometry data. The resistance of the 1 μm wire array through the phase transition at ZF is shown in figure 6. It can be seen that there is a shift in T_T for the OOP applied magnetic field with a drop
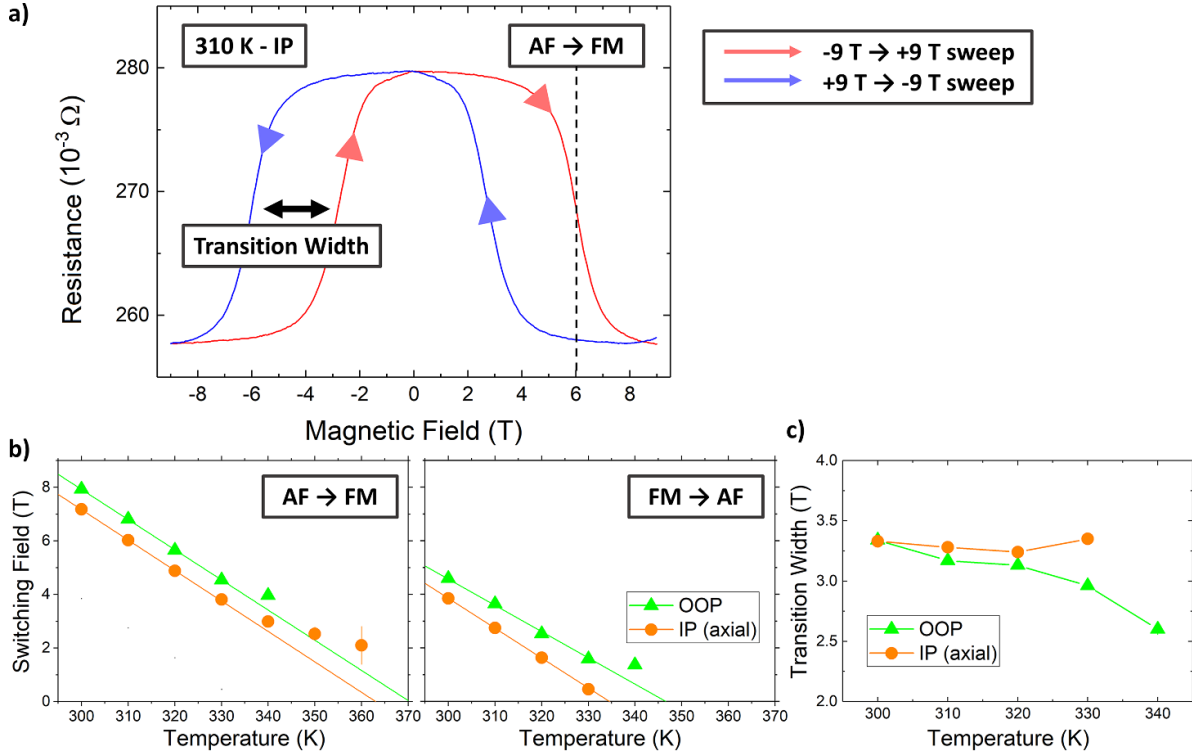
Figure 7. (a) Example of an isothermal field sweep where the resistance of a nanowire array (1 μm nanowire width) is measured at 310 K in an axial IP applied magnetic field. This is performed on changing the magnetic field both from $+9 \rightarrow -9$ T (blue curve), and $-9 \rightarrow +9$ T (red curve). The switching field is defined as the inflection point of the curve, where a decrease in resistivity is associated with the AF $\rightarrow$ FM transition and vice versa. These switching fields are averaged for the two sweep directions for each measured temperature. (b) The AF $\rightarrow$ FM (left plot) and FM $\rightarrow$ AF (centre plot) switching fields are plotted as a function of temperature for magnetic field applied IP and OOP. The difference in switching fields is assumed to be an indirect measure of the difference in internal magnetic field strength. The IP configuration is found to reduce the switching field in 1 μm nanowires by an average of 0.8 T.

of ≈ 3 K when compared to the temperature sweep performed to the ZF case. For the axial IP configuration, a larger shift in T_T is observed, up to 9 K. Similar shifts in T_T were also observed in 500 nm wires. The full set of transition parameters of the nanowire arrays extracted from these measurements are available in the supplementary material.

When comparing the transition temperatures for the axial IP magnetic field orientation to that obtained from the magnetometry data for an unpatterned film (see figure 1), no marked change in transition behaviour is observed. We therefore conclude the lithography procedure has not induced widespread structural disorder in the patterned samples [16]. Likewise, the similar transition properties of the 1 μm and 500 nm wire arrays indicate that strain relief due to nanoscale pattering has not measurably affected the transition properties. Having discounted a shift in the transition temperature, the changes in the TR-MOKE response for the nanowire arrays are therefore likely to be due to the shape anisotropy. However, in contrast to previous measurements on single wires [30], we do not observe a step-like FM $\rightarrow$ AF transition of the nanowire arrays during the IP measurements. One explanation for this is that transitions of individual FM domains to the AF phase cannot be observed when the response is averaged over the array [29]. However, it is seen that the transition is narrower for the IP magnetic field orientation when compared to the transition with an OOP field (ΔT of 12 compared with 15 K;

see supplementary material), which is evidence of FM phase stabilisation.

3.3.2. Resistance vs magnetic field curves. We next estimate the magnitude of the demagnetization fields, by measuring the applied field at which the AF $\rightarrow$ FM phase transitions occurs under different magnetic field orientations. The resistance is measured as the applied magnetic field is swept across ± 9 T for both axial IP and OOP magnetic field orientations. The width of the resistance versus magnetic field hysteresis loop, i.e. the difference between the fields at which the AF $\rightarrow$ FM and FM $\rightarrow$ AF transitions occur (see figure 7(a)), gives information on the stability of the FM phase, i.e. the wider the transition width, the more stable the FM phase is to the applied magnetic field. An example of an isothermal field sweep is provided in figure 7(a), where the transition width and AF $\rightarrow$ FM switching field are indicated on the resistance profiles. In figure 7(b), it can be seen how the FM phase of FeRh emerges at lower field strengths for an axial IP magnetic field at a given temperature (compare orange and green data). However, there is little evidence of phase asymmetry where the transition widths (given by the difference between AF $\rightarrow$ FM and FM $\rightarrow$ AF switching fields) are marginally increased for the IP versus OOP measurements (3.30 ± 0.05 versus 3.15 ± 0.16 T).

By considering the demagnetization fields, it is possible to explain the presence of field-stabilised FM phase under axial magnetic fields. Comparing the data for the two field configurations shown in figure 7(b) demonstrates that the IP field orientation reduces the transition field by 0.8 ± 0.1 T when compared to the OOP case. This is seen for both the AF $\rightarrow$ FM and FM $\rightarrow$ AF transitions (compare orange and green data). The 0.8 T reduction in the switching field of the FeRh nanowires, when the axial IP field results are compared to those performed with an OOP magnetic field, is consistent with the 7 K shift in T_T shown in figure 6(a), based on the empirical field dependence of T_T, which is reduced by 9 K T^{-1} [23, 51]. We attribute this change in behaviour to the shape anisotropy, as FeRh has only weak magnetic anisotropy as a result of its symmetric, cubic crystal structure [12, 39]. Calculating demagnetization factors based on the ratio of sample length to thickness and width [52], the coercive field, $\mathbf{H_C}$, of the wires can be determined as a function of angle. Assuming $\mathbf{H_C} < 30$ mT, for the FM FeRh [7] (see supplementary material), saturation along the wire lengths for the axial IP geometry is expected for applied field strengths < 40 mT. For an OOP geometry, magnetic fields of 1.1 T are required to saturate 1 μm. The predicted differences in the coercive fields for the axial IP and OOP magnetic field directions ($1.1 - 0.04$ T) are similar to the experimentally determined difference in switching field (0.8 T). This indicates that measuring switching fields under different field orientations is a suitable estimate of the demagnetisation field strengths.

Having determined the difference in demagnetization fields for axial IP and OOP applied fields, we now try to explain the observed behaviour of the Kerr remanence signal, Θ_R, in nanowire arrays under a tangential field shown in figure 4. The electrical measurements show that changing the applied magnetic field from OOP to IP, results in a change in the T_T of 6 K (figure 6(a)), which is not sufficient to explain the strong divergence in behaviour seen when comparing axial (figure 3) and tangential (figure 4). Based on the finite-element modelling simulations and previous studies [33], a laser pulse with a fluence of 4.0 mJ cm^{-2}, is expected to induce a temperature rise of > 150 K. As such, the excited sample will transition to the fully FM state, irrespective of field direction. However, the demagnetisation field strength as a function of angle offers a more plausible argument. As seen from the rapid rise in Kerr signal in both figures 3 and 4, the field orientation does not measurably affect the initial formation of the FM phase, which is induced by fs laser heating within 30 ps. This is consistent with recent x-ray absorption spectroscopy studies [47] where small FM regions are observed within a few ps. We propose that the decreased demagnetization field, when an axial IP magnetic field is applied, promotes the field alignment of the magnetization of the laser-induced FM domains. With the field strengths used (110 mT), the FeRh nanowires are saturated by an axial field ($\mathbf{H_C} < 50$ mT) but not by a tangential field ($\mathbf{H_C} > 200$ mT). The subsequent inability for the tangential field to saturate the wires along the field direction would explain the reduced Kerr remanence signal in figure 4 compared to figure 3. Indeed, the nanowire arrays show a long-lived remanence signal under an axial field, and a weak remanence signal under a tangential field. Furthermore, the lifetime of the remanence signal is observed to increase under an axial field when compared to the same experiments performed on thin films. The field-aligned FM regions within the FeRh nanowires relax more slowly when the demagnetising field is minimised. Such a metastable FM state in FeRh nanowires has previously been observed by Uhlíř *et al* [30], where it was argued that the lower demagnetisation field stabilised field-aligned FM domains. Using electrical measurements, these authors observed an FM phase in 500 nm wide wires at lower than expected temperatures (reduction of 10 K) using axial magnetic fields of similar strengths. Recently, memristive properties have been observed in FeRh nanopillars of 300 nm width [53], with potential applications as artificial synapses. The ability to control the lifetime of laser-induced FM phase offers a method to engineer similar nanostructures for neuromorphic applications.

4. Conclusions

We probed the transient ferromagnetism in Fe$_{50}$Rh$_{50}$ thin films and nanowire array samples by measuring TR-MOKE as a function of applied magnetic field, and obtained the Kerr remanence signals as a function of time. Following fs laser excitation in an axial field, the onset of ferromagnetism appears to be similar for thin films and nanowire arrays, with comparable growth lifetimes for the remanent Kerr signal, Θ_R, of $\approx$75 ps. In contrast, the FM phase is found to persist for longer times in nanowire arrays than in the thin films. This indicates that there is an increased FM stability in the nanowires, which has previously been reported in static measurements, and leads to a slower relaxation to the AF phase on the ns timescale.

Comparing the results for an axial IP magnetic field with those for a tangential field, a transient Kerr response is observed with a much increased remanence, Θ_R, in the nanowire arrays with an axial magnetic field, indicating how increased internal fields stabilise the FM domains. Furthermore, the total Kerr response was observed to relax more slowly under axial applied fields. When the transition temperature, T_T, of individual nanowire arrays was determined using four-point probe measurements of the resistance as a function of temperature, it was found that T_T did not change after patterning the thin films into nanowires. However, we did find that T_T is sensitive to the direction of applied magnetic field (1 T) for the nanowire arrays, being reduced by 6 K when field is applied axially IP as opposed to OOP. Estimation of the effective fields within nanowire arrays indicate that, when going from an OOP to an IP magnetic field, there is an increase in the internal field strength by up 0.8 T. We therefore attribute the increased stability of the FM phase to this larger internal field.

J. Phys. D: Appl. Phys. **56** (2023) 485002

M Grimes *et al*

In order to ensure that heat dissipation is not responsible for the observed FM phase stabilisation, we developed a finite-element model using COMSOL® to estimate the sample temperature following laser excitation in both thin films and nanowire arrays and found that there is no indication that nanowire arrays have a reduced ability to dissipate heat during these pumped laser experiments. We have therefore demonstrated that shape anisotropy is a key factor that influences the phase transition where demagnetization fields within nanowires stabilises the FM phase and reduces the energy barrier of the AF → FM transition. Thus the relaxation times of laser-induced FM regions can be controlled by modifying the orientation and magnitude of the applied magnetic field as well as the aspect ratio of the nanowires. Indeed, by changing the applied IP magnetic field from tangential to axial for the thinnest nanowires, the relaxation times can be increased by a factor of 2. This should be taken into account when implementing FeRh in high frequency HAMR applications, becoming particularly important as the FeRh elements in the devices are reduced in size. The ability to control FM lifetimes is also of particular interest for memristive applications, such as in neuromorphic computing.

Data availability statement

Acknowledgments

ORCID iDs

M Grimes https://orcid.org/0000-0001-8000-923X
S Parchenko https://orcid.org/0000-0002-4320-4957
L J Heyderman https://orcid.org/0000-0003-3843-6611
T Thomson https://orcid.org/0000-0002-4110-1567
V Scagnoli https://orcid.org/0000-0002-8116-8870

References

[1] Vedmedenko E Y *et al* 2020 The 2020 magnetism roadmap *J. Phys. D: Appl. Phys.* **53** 453001
[2] McDaniel T W 2005 Ultimate limits to thermally assisted magnetic recording *J. Phys.: Condens. Matter* **17** 315–32
[3] Rea C *et al* 2016 Areal-density limits for heat-assisted magnetic recording and perpendicular magnetic recording *IEEE Trans. Magn.* **52** 1–4
[4] Thiele J U, Maat S and Fullerton E 2003 FeRh/FePt antiferromagnet/ferromagnet exchange spring media for thermally assisted magnetic recording *Appl. Phys. Lett.* **82** 2859
[5] Fallot M 1938 Les alliages du fer avec les métaux de la famille du platine *Ann. Phys.* **11** 291–332
[6] Kouvel J S 1966 Unusual nature of the abrupt magnetic transition in FeRh and its pseudobinary variants *J. Appl. Phys.* **37** 1257–8
[7] Kouvel J S and Hartelius C C 1962 Anomalous magnetic moments and transformations in the ordered alloy FeRh *J. Appl. Phys.* **33** 1343
[8] Ricodeau J A and Melville D 1972 Model of the antiferromagnetic-ferromagnetic transition in FeRh alloys *J. Phys. F* **2** 337–50
[9] Stamm C *et al* 2008 Antiferromagnetic-ferromagnetic phase transition in FeRh probed by x-ray magnetic circular dichroism *Phys. Rev. B* **77** 184401
[10] Baranov N V and Barabanova E A 1995 Electrical resistivity and magnetic phase transitions in modified FeRh compounds *J. Alloys Compd.* **219** 139–48
[11] Zsoldos L 1967 Lattice parameter change of FeRh alloys due to antiferromagnetic–ferromagnetic transformation *Phys. Status Solidi* **20** 25–28
[12] Kren E, Pal L and Szabo P 1964 Neutron diffraction investigation of the antiferromagnetic–ferromagnetic transformation in the FeRh alloy *Phys. Lett.* **9** 297–8
[13] Lewis L H, Marrows C H and Langridge S 2016 Coupled magnetic, structural, and electronic phase transitions in FeRh *J. Phys. D: Appl. Phys.* **49** 323002
[14] Jiménez M J, Schvval A B and Cabeza G F 2020 Ab initio study of FeRh alloy properties *Comput. Mater. Sci.* **172** 109385
[15] Pressacco F *et al* 2021 Subpicosecond metamagnetic phase transition in FeRh driven by non-equilibrium electron dynamics *Nat. Commun.* **12** 5088
[16] Eggert B *et al* 2020 Magnetic response of FeRh to static and dynamic disorder *RSC Adv.* **10** 14386–95
[17] Barton C W, Ostler T A, Huskisson D, Kinane C J, Haigh S J, Hrkac G and Thomson T 2017 Substrate induced strain field in FeRh epilayers grown on single crystal MgO (001) substrates *Sci. Rep.* **7** 44397
[18] Baldasseroni C *et al* 2014 Effect of capping material on interfacial ferromagnetism in FeRh thin films *J. Appl. Phys.* **115** 43919
[19] Loving M G, Barua R, Le G C, Kinane C J, Heiman D, Langridge S, Marrows C H and Lewis L H 2018 Strain-tuning of the magnetocaloric transition temperature in model FeRh films *J. Phys. D: Appl. Phys.* **51** 024003
[20] Ostler T A, Barton C, Thomson T and Hrkac G 2017 Modeling the thickness dependence of the magnetic phase transition temperature in thin FeRh films *Phys. Rev. B* **95** 1–7
[21] Griggs W *et al* 2020 Depth selective magnetic phase coexistence in FeRh thin films *APL Mater.* **8** 121103
[22] Bull C, Barton C W, Griggs W, Caruana A, Kinane C J, Nutter P W and Thomson T 2019 PNR study of the phase transition in FeRh thin films *APL Mater.* **7** 101117
[23] Song S *et al* 2023 Vertical inhomogeneous magnetic order in FeRh film *Appl. Surf. Sci.* **607** 154870
[24] Bennett S P, Herklotz A, Cress C D, Ievlev A, Rouleau C M, Mazin I and Lauter V 2018 Magnetic order multilayering in FeRh thin films by He-ion irradiation *Mater. Res. Lett.* **6** 106–12
[25] Inoue S, Ko H Y Y and Suzuki T 2008 Magnetic properties of single-crystalline FeRh alloy thin films *IEEE Trans. Magn.* **44** 2875–8
[26] Mcgrath B, Camley R E and Livesey K L 2020 Self-consistent local mean-field theory for phase transitions and magnetic properties of FeRh *Phys. Rev. B* **101** 014444

J. Phys. D: Appl. Phys. **56** (2023) 485002

M Grimes *et al*

[27] Sandratskii L M and Mavropoulos P 2011 Magnetic excitations and femtomagnetism of FeRh: a first-principles study *Phys. Rev. B* **83** 174408

[28] Temple R C *et al* 2018 Antiferromagnetic-ferromagnetic phase domain development in nanopatterned FeRh islands *Phys. Rev. Mater.* **104406** 1–9

[29] Warren J L, Barton C W, Bull C and Thomson T 2020 Topography dependence of the metamagnetic phase transition in FeRh thin films *Sci. Rep.* **10** 4030

[30] Uhlíř V, Arregi J A and Fullerton E E 2016 Colossal magnetic phase transition asymmetry in mesoscale FeRh stripes *Nat. Commun.* **7** 13113

[31] Radu I, Stamm C, Pontius N, Kachel T, Ramm P, Thiele J U, Dürr H A and Back C H 2010 Laser-induced generation and quenching of magnetization on FeRh studied with time-resolved x-ray magnetic circular dichroism *Phys. Rev. B* **81** 104415

[32] Thiele J-U-U, Buess M and Back C H 2004 Spin dynamics of the antiferromagnetic-to-ferromagnetic phase transition in FeRh on a sub-picosecond time scale *Appl. Phys. Lett.* **85** 2857–9

[33] Grimes M *et al* 2022 Determination of sub-ps lattice dynamics in FeRh thin films *Sci. Rep.* **12** 8584

[34] Awari N *et al* 2020 Monitoring laser-induced magnetization in FeRh by transient terahertz emission spectroscopy *Appl. Phys. Lett.* **117** 122407

[35] Ünal A A, Parabas A, Arora A, Ehrler J, Barton C, Valencia S, Bali R, Thomson T, Yildiz F and Kronast F 2017 Laser-driven formation of transient local ferromagnetism in FeRh thin films *Ultramicroscopy* **183** 104–8

[36] Baldasseroni C, Bordel C, Gray A X, Kaiser A M, Kronast F, Herrero-Albillos J, Schneider C M, Fadley C S and Hellman F 2012 Temperature-driven nucleation of ferromagnetic domains in FeRh thin films *Appl. Phys. Lett.* **100** 262401

[37] Baldasseroni C, Bordel C, Antonakos C, Scholl A, Stone K H, Kortright J B and Hellman F 2015 Temperature-driven growth of antiferromagnetic domains in thin-film FeRh *J. Phys.: Condens. Matter* **27** 256001

[38] Grimes M, Gurung N, Ueda H, Porter D G, Pedrini B, Heyderman L J, Thomson T and Scagnoli V 2022 X-ray investigation of long-range antiferromagnetic ordering in FeRh *AIP Adv.* **12** 035048

[39] Mancini E, Pressacco F, Haertinger M, Fullerton E E, Suzuki T, Woltersdorf G and Back C H 2013 Magnetic phase transition in iron-rhodium thin films probed by ferromagnetic resonance *J. Phys. D: Appl. Phys.* **46** 245302

[40] Le G C, de Vries M A, McLaren M, Brydson R M D, Loving M, Heiman D, Lewis L H and Marrows C H 2013 Sputter growth and characterization of metamagnetic B2-ordered FeRh epilayers *J. Vis. Exp.* **80** 1–8

[41] Riahi H, Thevenard L, Maaref M A, Gallas B, Lemaître A and Gourdon C 2015 Optimizing magneto-optical effects in the ferromagnetic semiconductor GaMnAs *J. Magn. Magn. Mater.* **395** 340–4

[42] Hunt R P 1967 Magneto-optic scattering from thin solid films *J. Appl. Phys.* **38** 1652

[43] Li S, Chen Z, Cheng C, Li J, Zhou S and Lai T 2013 Coercivity dynamics and origin of time-delayed magneto-optical hysteresis loops in pump-probe Kerr spectroscopy *J. Appl. Phys.* **113** 53913

[44] Humaish H 2020 Evaluating a line heat source method using a COMSOL® multiphysics axisymmetric 2D model *IOP Conf. Ser.: Mater. Sci. Eng.* **671** 012088

[45] Zuo S, Nazarpour K and Heidari H 2018 Device modeling of MgO-barrier tunneling magnetoresistors for hybrid spintronic-CMOS *IEEE Electron Device Lett.* **39** 1784–7

[46] Mariager S O *et al* 2012 Structural and magnetic dynamics of a laser induced phase transition in FeRh *Phys. Rev. Lett.* **108** 087201

[47] Li G, Medapalli R, Mentink J H, Mikhaylovskiy R V, Blank T G H, Patel S K K, Zvezdin A K, Rasing T, Fullerton E E and Kimel A V 2022 Ultrafast kinetics of the antiferromagnetic–ferromagnetic phase transition in FeRh *Nat. Commun.* **13** 1–9

[48] Oblak E, Riego P, Fallarino L, Martínez-De-Guerenu A, Arizti F and Berger A 2017 Ultrasensitive transverse magneto-optical Kerr effect measurements by means of effective polarization change detection *J. Phys. D: Appl. Phys.* **50** 23–24

[49] Agarwal N 2022 Ultrafast dynamics of electronic structure and domain nucleation during photo-induced phase transition in FeRh (European x-ray Free-Electron Laser Facility GmbH)

[50] Stoner E C and Wohlfarth E P 1948 A mechanism of magnetic hysteresis in heterogeneous alloys *Phil. Trans. R. Soc. A* **240** 599–642

[51] Nam N T, Lu W and Suzuki T 2009 Temperature dependence of magnetic properties in epitaxial FePt/FeRh bilayer *IEEE Trans. Magn.* **45** 2531–3

[52] Osborn J A 1945 Demagnetizing factors of the general ellipsoid *Phys. Rev.* **67** 351–7

[53] Temple R C, Rosamond M C, Massey J R, Almeida T P, Linfield E H, McGrouther D, McVitie S, Moore T A and Marrows C H 2021 Phase domain boundary motion and memristance in gradient-doped FeRh nanopillars induced by spin injection *Appl. Phys. Lett.* **118** 122403